Colloids and Surfaces A: Physicochemical and Engineering Aspects 661 (2023) 130807

Contents lists available at ScienceDirect

Colloids and Surfaces A: Physicochemical and Engineering Aspects

journal homepage: www.elsevier.com/locate/colsurfa

Mammalian cell encapsulation in monodisperse chitosan beads using microchannel emulsification

Dongjin S. Shin [a], Francesco K. Touani [c,d], Damon G.K. Aboud [a], Anne-Marie Kietzig [a], Sophie Lerouge [c,e,*], Corinne A. Hoesli [a,b,**]

[a] Department of Chemical Engineering, McGill University, Montreal, Canada
[b] Department of Biomedical Engineering, McGill University, Montreal, Canada
[c] Laboratory of Endovascular Biomaterials (LBeV), Centre de recherche du CHUM, Montreal, Canada
[d] Department of Pharmacology and Physiology, University of Montreal, Montreal, Canada
[e] Department of Mechanical Engineering, École de technologie supérieure (ÉTS), Montreal, Canada

GRAPHICAL ABSTRACT

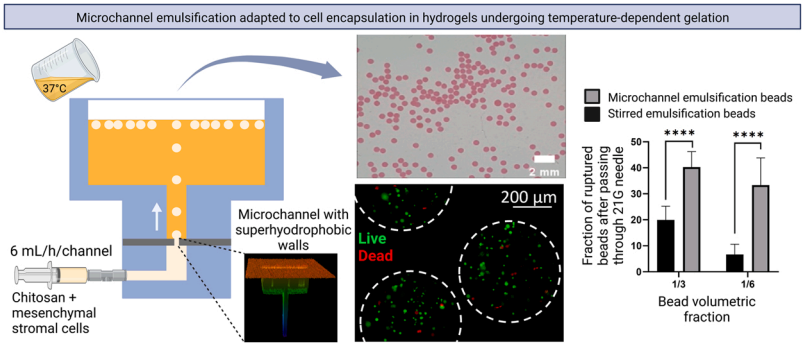

ARTICLE INFO

Keywords:
Microchannel emulsification
Encapsulation
Thermoresponsive
Hydrogel
Chitosan
Mesenchymal stromal cells

ABSTRACT

Microchannel emulsification can produce droplets of uniform size at high throughput for wide-ranging applications in the food and drug industry. Mammalian cell encapsulation using emulsion-based systems is of significant interest for immobilized culture or transplantation applications. Microchannel emulsification has recently been applied to mammalian cell encapsulation using alginate. Here, we extend this approach to thermoresponsive hydrogels using chitosan as a model. The performance of the microchannel emulsification process was compared to a previously established stirred emulsification method for mesenchymal stromal cell encapsulation. Chitosan microbeads with controlled sizes ranging from 600 µm to 1500 µm in diameter at a coefficient of variation less than 10 % were obtained after adapting the microchannel system design, channel geometries and operating parameters that affect the capillary number. In a single pass through a 21 G syringe needle, the fraction of ruptured beads was significantly reduced for monodisperse microchannel-generated vs polydisperse stirred emulsion-generated beads of matching De Brouckere mean diameter. The viability of the immobilized cells immediately after the process was 95 % ± 2 % and no significant difference in cell survival and growth

* Correspondence to: Department of Mechanical Engineering, École de technologie supérieure (ÉTS), 1100 Notre-Dame West, Montreal, Québec H3C 1K3, Canada.
** Correspondence to: Department of Chemical Engineering, McGill University, 3610 rue University, Montreal, Québec H3A 0C5, Canada.
E-mail addresses: sophie.lerouge@etsmtl.ca (S. Lerouge), corinne.hoesli@mcgill.ca (C.A. Hoesli).

https://doi.org/10.1016/j.colsurfa.2022.130807
Received 22 October 2022; Received in revised form 7 December 2022; Accepted 16 December 2022
Available online 22 December 2022

factor secretion was observed between microchannel and stirred emulsion-generated beads over 3 days of culture. Microchannel emulsification is a promising and scalable approach to microencapsulate mammalian cells in hydrogels that undergo temperature-dependent gelation.

1. Introduction

Mammalian cell encapsulation in hydrogels has gained significant traction for immobilized culture and transplantation applications. Compared to nozzle-based encapsulators [1], emulsion-based cell encapsulation methods have the advantage of producing highly spherical droplets and being more readily amenable to scale-up or parallelization. Emulsion-based cell encapsulation methods have implemented either stirred systems that can readily be upscaled but produce polydisperse beads [2–5], or microfabricated devices that produce monodisperse droplets at limited throughput [6–10].

Microchannel emulsification, also termed step emulsification, is geometry-driven method of producing monodisperse droplets using symmetric [11] or asymmetric oblong channels. Droplet detachment is driven by hydrodynamic instability of the dispersed phase as it flows from the confined microchannel into an expanding space filled with continuous phase fluid [12,13]. The dispersed phase flow rate mainly affects droplet formation frequency rather than diameter below a critical capillary number value (Ca_c) [14,15]. Contrary to membrane emulsification, droplet detachment does not depend on or require continuous phase crossflow. This leads to highly robust droplet production irrespective of disturbances in flow conditions that would affect other membrane or microfluidic droplet production systems. Microchannels can be parallelized to increase throughput while requiring much lower energy input than other scale-up methods such as high-pressure or ultrasonic homogenizers [11,16,17]. To our knowledge, microchannel emulsification has so far only been applied to mammalian cell encapsulation in alginate – either via external [18] or internal [19] ionotropic gelation. There is significant interest in extending this approach to other hydrogels commonly used for mammalian cell culture or transplantation, many of which are thermoresponsive [20]. For applications requiring cell release from the microbeads, bioresorbable polymers are preferred over alginate which is not readily degraded by endogenous human enzymes.

Chitosan, an amino-polysaccharide obtained by deacetylation of chitin [21], is of particular interest in controlled delivery of drugs as well as living cells due to its tunable degradation rate. While most solubilization methods require acidification which is problematic for cell processing [22], adding a weak base to the solubilized chitosan solution prior to mixing with cells can generate a cytocompatible chitosan solution which undergoes accelerated sol-gel transition at body temperature [23]. Formulations that combine sodium hydrogen carbonate with beta-glycerophosphate or phosphate buffer show significant promise as an injectable gel for the delivery of therapeutic cells such as mesenchymal stromal cells (MSCs) [24,25]. *In situ* injection of MSC-loaded chitosan pre-gel creates macrogels which introduce a diffusion barrier for oxygen as well as pro-angiogenic and immunosuppressive factors secreted by MSCs. Maximizing the surface area/volume ratio through delivery of microencapsulated MSCs could favour graft survival, engraftment and therapeutic effect.

The goal of this project was to adapt the microchannel emulsification system to cell encapsulation in chitosan hydrogels which undergo temperature-sensitive sol-gel transition. A microchannel emulsification setup previously applied to alginate-based cell immobilization was modified to reduce dead volume and introduce a temperature change. The effect of process parameters such as addition of emulsifier, channel geometry, chitosan concentration and flow rate on the resulting bead diameter was studied while relating findings to the predicted capillary number (Ca). The resulting process conditions can generate beads of 600 – 1500 μm in diameter at a coefficient of variation of less than 10 %. When compared to stirred emulsification, no significant differences in bead mechanical properties, MSC survival or secretory profiles were observed in vitro. The injectability of the microchannel microbeads was significantly improved over beads produced by stirred emulsification when passing through a needle of internal diameter near the bead volume-average diameter. Microchannel emulsification of hydrogels that undergo temperature-dependent gelation such as chitosan is a promising approach for scalable mammalian cell encapsulation.

2. Materials and methods

2.1. Hydrogel preparation

Shrimp shell chitosan powder (ChitoClear, HQG110, M_w: 150–250 kDa, degree of deacetylation 93 %, Primex Iceland) was solubilized in 0.12 M HCl solution using an overhead stirrer at 900 rpm for three hours. This solution was sterilized by autoclaving for 20 min at 121 °C, 15 psi. The gelling agent solution was a mixture of two weak bases: sodium hydrogen carbonate $NaHCO_3$ (G9422, Sigma-Aldrich) and phosphate buffer [25]. Phosphate buffer solution was prepared at 0.1 M (pH 8.0) by solubilizing sodium phosphate dibasic Na_2HPO_4 (S5136, Sigma-Aldrich) and sodium phosphate monobasic NaH_2PO_4 (S2554, Sigma-Aldrich) in Milli-Q water at 2.65×10^{-2} g/mL and 0.16×10^{-2} g/mL, respectively. Then, sodium hydrogen carbonate was solubilized in phosphate buffer solution at 0.375 M. The pH of the gelling agent was measured using a pH meter (LAQUAtwin pH-22, Horiba). The gelling agent solution (phosphate buffer 0.1 M; sodium hydrogen carbonate 0.375 M) was passed through a 0.22 μm filter (Corning) for sterilization [5]. Chitosan solution and gelling agent were mixed at 3:1 volumetric ratio using syringes and a Female Luer lock connector before adding the cell stock (for experiments with cells) or cell-free medium at 4:1 volumetric ratio. The resulting chitosan precursor solution formulation contained 0.02 M phosphate buffer, 0.075 M sodium hydrogen carbonate and 0.5×10^6 cells/mL. The serum-free medium used for encapsulation was alpha minimum essential medium (alpha-MEM, Gibco) supplemented with 0.75 % bovine serum albumin (BSA, A4812, Sigma-Aldrich).

2.2. Cell culture/Cell stock preparation

Bone marrow derived human MSCs (Lonza) were cultured using NutriStem XF medium supplemented with 0.6 % MSC NutriStem XF Supplement (Biological Industries), a xeno-free and defined medium. Cells were seeded at 2860 cell/cm^2 density on T175 tissue culture flasks (Canted Neck Red Ventilated Cap for Adherent Cells, 50–809–259, SARSTEDT) with medium volumes of 0.142 mL/cm^2 and passaged upon reaching 90 % confluence based on microscope observation. Immediately before encapsulation, the cells were detached with 0.03 mL/cm^2 of Trypsin/EDTA (Wisent) and incubated for 3–5 min. Then, the cell suspension was transferred into a 50 mL conical tube and centrifuged at 500 x g for 5 min. The cells were re-suspended in alpha-MEM + 0.75 % BSA at 5-fold the desired final cell concentration in chitosan hydrogel.

2.3. Interfacial tension measurement

The interfacial tension between the oil phase and the chitosan was measured at room temperature by the pendant drop method using a goniometer (Future Digital Scientific) connected to a video camera system and computer software (SCA20, Dataphysics). A quartz cuvette was filled with chitosan solution. A 500 μL syringe needle (523159,

Hamilton) filled with oil was immersed into the solvent and a droplet was created by ejection at 36 μL/s. The drop profile of the oil phase suspended in the chitosan solution was recorded using a high-speed camera. The interfacial tension was estimated by fitting the Young-Laplace equation to experimental images using OpendropV1.1 software (Supporting Information) [26]. For the fitting process, the differences in density of the liquids were considered (chitosan mixture density of 1.1 g/cm^3; Novec oil density of 1.614 g/cm^3). For each sample solution, the interfacial tension value was the average of three measurements.

2.4. Viscosity measurement

The apparent viscosity of the chitosan precursor solution was measured at room temperature (~22 °C) using a MCR302 Rheometer (Anton Paar) with a cone-plate system (strain and frequency at 1 % and 1 Hz, respectively) immediately after mixing. Shear rate was ramped logarithmically from 0.1 s^{-1} to 200 s^{-1} for a total of 15 s. The inspection time was 1 s and the duration of inspection was 0.5 s for each data point. Milli-Q water was used for the precursor solution preparation instead of gelling agent to avoid viscosity changes during the measurement.

2.5. Microchannel device & channel fabrication

The device consists of a microchannel plate sandwiched between a bottom and top chamber designed to be easily assembled/disassembled (Supporting Information Fig. S1). The top and bottom chambers were designed using AutoCAD (AutoDesk©) software and machined from acrylic rods (8528K55, Clear Scratch- and UV-Resistant Cast Acrylic Rod, 4–1/2" Diameter, McMaster-Carr). Microchannels were machined from polytetrafluoroethylene (PTFE) sheets (9266K11, Chemical-resistant slippery PTFE Sheets, McMaster-Carr) of either 1.635 mm or 0.86 mm in thickness via femtosecond laser micromachining. The laser setup consists of a Libra Ti: Sapphire laser system (Coherent) with a central wavelength of 800 nm, pulse duration < 100 fs, and a 1 kHz repetition rate. The pulse energy used was 200 μJ, and the beam was focused using a 200 mm focal length convex lens to a spot radius of 20 μm, leading to a pulse peak fluence of 30.7 J/cm^2. The surface was micromachined in a raster scanning pattern using a translation speed of 2 mm/s and a line spacing of 20 μm. High resolution 3D images of the channels were acquired using a laser confocal microscope (Olympus OLS 4000 LEXT).

2.6. Dynamic contact angle measurement

Water contact angles were measured by dispensing 2 μL reverse osmosis water droplets on test surfaces using a 32 G syringe needle (Hamilton). Then, the liquid volume was increased to 7 μL at a rate of 0.25 μL/s. After a five second pause, all the liquid was drawn back into the needle. The advancing and receding contact angles of the resulting videos were measured using SCA20 software (DataPhysics Instruments).

2.7. Scanning electron microscopy

PTFE surfaces were sputter-coated with platinum to develop a 5 nm thick conductive layer on the surface using an EM ACE600 sputter coater (Leica). Images were acquired using a Quanta 450 scanning electron microscope (FEI company).

2.8. Microbead production by microchannel emulsification

The bottom chamber inlet port was connected (1/16" tube to male threaded connector, 5117K85, with O-ring seal 5233T474, McMaster-Carr) to 5 cm length Tygon tubing (Saint-Gobain) with a female Luer to hose barb connector at the other extremity. Two O-rings were placed in grooves located (a) between the microchannel plate and the top chamber and (b) between the microchannel plate and the bottom chamber to create a water-tight seal (Supporting Information Fig. S1). The microchannel plate was placed between the top chamber and the bottom chamber and devices were assembled using four tightening screws (Fig. 1. A). For cell culture experiments, device components were sterilized through overnight immersion in a 70 % ethanol bath and air-drying for 30 min in a biosafety cabinet followed by aseptic handling. The chitosan precursor solution was prepared in a syringe with the desired volume (3–5 mL, Beckton-Dickinson) which was then mounted onto the syringe pump (Sage Instruments mode 355/365, Cole-Parmer) (Fig. 1. B). To prepare the oil phase for microchannel emulsification, FluoroSurfactant (RAN Biotechnologies in HFE7500, catalogue #008-FluoroSurfactant-5wtH-20 G) was dissolved in 3 M™ Novec™ 7500 (3 M Company) at 0.066 % w/w and aseptically filtered (0.2 μm syringe filters, SARSTEDT). A total of 70 mL of oil phase was prepared per batch. Out of 70 mL, 50 mL was preheated to 37 °C, and the rest (20 mL) was stored at 22 °C. Then, the aqueous phase was infused into the bottom chamber until the solution level reached the microchannel plate (1 ~ 1.5 mL). To promote rapid gelation at the oil surface but avoid early gelation at the interface, 20 mL of the 22 °C oil was poured into the top chamber followed by gradual addition of 50 mL of the 37 °C oil (Fig. 1. B). While the preheated oil was slowly being added, the aqueous phase was pumped into the bottom chamber, initially with a flow rate of 1 mL/min to purge air trapped inside the channel, which was steadily decreased to the desired flow rate for droplet production. The droplets detached from the microchannel floated to the oil surface. When the desired volume of droplets was obtained at the collection site, the top was sealed with ethanol-sterilized parafilm and the entire device was placed in an incubator to ensure complete gelation at 37 °C for an additional 5 − 10 min. Then, the device was taken out of the incubator and 10 mL of HEPES-buffered saline solution (10 mM 4-(2-hydroxyethyl)− 1-piperazineethanesulfonic acid, 170 mM NaCl, pH 7.4 – all from Sigma-Aldrich – supplemented with 10% serum-free medium consisting of alpha-MEM + 0.75% BSA) was added into the collection chamber. The fully gelled chitosan microbeads were transferred to a 100 μm nylon cell strainer (22363–549, Fisher) using a spatula and rinsed by evenly dispensing 5 10- 15 mL of HEPES-buffered saline solution over the beads. Microbeads were resuspended with alpha-MEM containing 10% FBS to a ratio of 1:1 (v/v). A volume of 200 μL of beads suspension were transferred to a 24well plate (9023511, SARSTEDT) and 800 μL of low-serum medium (0.2 % FBS in alpha-MEM) were added to each well plate. Half of the beads were used for cell viability measurements immediately after the encapsulation and the other half were cultured in low-serum medium for 3 days.

2.9. Microbead production by stirred emulsification

Chitosan microbeads were generated via stirred emulsification as previously described [5]. Briefly, 20 mL of light mineral oil (O121–4, Fisher) was placed in a 50 mL microcarrier spinner flask (Bellco) located in a preheated in water bath (37 °C). The water bath was placed on a magnetic stirrer (VWR). With continual agitation at 600 rpm, the aqueous phase was prepared as mentioned above (3 mL) and injected into the preheated oil through a 18 G syringe needle (1" in length, Air-Tite) drop by drop immediately after chitosan preparation. At the 3-min mark, the rotational speed was gradually decreased to 200 rpm and beads were left to gel for 7 min at this mixing speed. At the 10-min mark, 50 mL of HEPES-buffered saline solution was added. The beads were separated from the oil, washed and transferred to 24-well plates as described for microchannel emulsification. The impeller rotational speed (600 rpm) was determined to match De Brouckere mean diameter ($D_{4,3}$, also called volume-weighted mean diameter) of the microchannel emulsification beads.

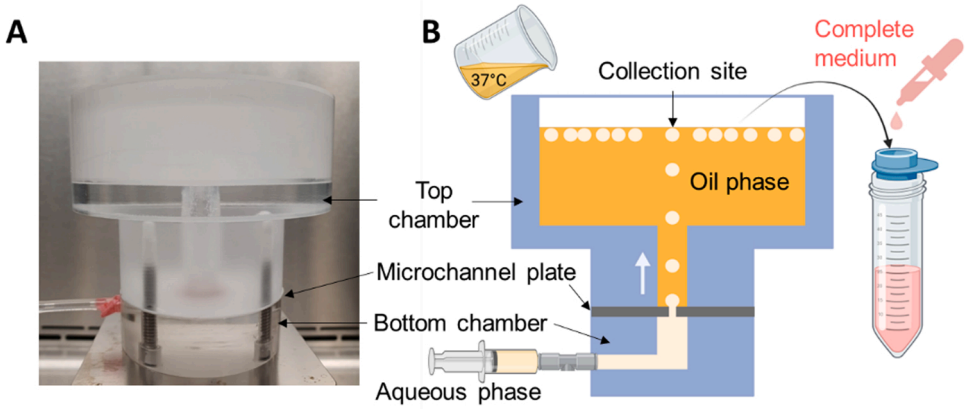

Fig. 1. Microchannel emulsification device and the microbead production process. (**A**) photograph of the microchannel device. (**B**) Schematic drawing of the encapsulation method using the microchannel emulsification device created using BioRender.com.

2.10. Microbead size and size distribution

Beads (0.5 mL) were placed in 10 mL of 0.01 g/L Eosin Y (Fisher Chemicaltm) in HEPES-buffered saline solution. The solution was stirred for 20 min on a rotary shaker. Images of stained beads were acquired using an UVP Biospectrum Imaging system. The diameter equivalent to the surface area in 2D images was determined using the analyze particles function in ImageJ [27]. The $D_{4,3}$ [2,4] and coefficient of varication (C.V.) were calculated from the diameter distributions of each batch using JMP (SAS) software.

2.11. Bead mechanical properties

The microbead mechanical properties and viscoelasticity were assessed using a MicroSquisher (CellScale) with a parallel-plate compression configuration and a 305 μm diameter microbeam as previously described [5]. Hand-picked microbeads of 700 – 800 μm diameter were placed onto a metal platform immersed in HEPES buffered saline solution at room temperature. Each bead went through three consecutive cycles of up to 30 % volume compression (30 s loading time, 10 s hold time, 30 s recovery time) to measure the force as a function of displacement using the accompanying software (SquisherJoy). The compressive modulus (E) of each microbead was calculated using the modified Hertzian half-space contact model (Supporting Information) [28].

2.12. Injectability

Cell-free microbeads of matching $D_{4,3}$ were generated using microchannel and stirred emulsification. Microbeads (1 mL) were suspended in HEPES-buffered saline solution at different dilutions (3 mL and 6 mL). Bead suspensions (total of 200 μm) were pipetted and transferred to a syringe (1 mL) and the beads were manually (to reproduce handling for animal or clinical studies) injected through 21 G (inner diameter 513 μm) needles (305167, BD) in 24 wells plate filled with 500 μL HEPES-buffered saline solution. Images were taken using phase-contrast light microscopy (Leica DM LB2) to quantify the number of ruptured or damaged beads.

2.13. Viability of immobilized MSCs

Each sample of 200 μL bead suspension was transferred to a well (24-well plates) followed by the addition of 500 μL alpha-MEM +0.75 % BSA containing 2 μM Calcein AM and 5.5 μM ethidium homodimer. After 45 min incubation, live/dead images were taken randomly at five different locations per sample with an inverted fluorescence microscope (Leica DMIRB) at 50x magnification. The images were analyzed using ImageJ (threshold/analyze/analyse particle) [27].

2.14. Paracrine activity

The paracrine activity of the cells was assessed by measuring the concentration of vascular endothelial growth factor A (VEGF) released in the conditioned media (0.2 % FBS in alpha-MEM) of micro-encapsulated MSCs (5×10^5 cells/mL) after 3 days of incubation. Conditioned media samples were centrifuged (5 min, 390 x g) to remove cell and gel debris, then diluted 1/3 in fresh medium (0.2 % FBS in alpha-MEM)The amount of VEGF was determined using the Quantikine ELISA Human VEGF Immunoassay (Biotechne).

2.15. Statistics

Normality tests were conducted. For data with normal distribution, two-way comparisons were performed using t-tests. Multiple comparisons used two-way ANOVA (GraphPad Prism 9.4.0) followed by Tukey post-hoc tests. For non-normal distributions, two-way comparisons were performed using Mann-Whitney tests. The level of significance was determined based on p-value (ns = $p > 0.05$, *: $p < 0.05$). Results with replicates were represented as average ± standard error of the mean (GraphPad Prism 9.4.0). N represents the number of replicates and n represents the number of samples in each replicate batch.

3. Process development and results

The main challenges in encapsulating MSCs in chitosan beads via microchannel emulsification were to assure sufficiently rapid bead gelation to avoid coalescence in the collection bath, and to obtain microbeads that were small enough to be injectable. An iterative process was applied to identify an appropriate surfactant addition method, device design and microchannel geometry.

3.1. Channels on the order of 200 μm created through thick plates

To determine the effect of channel geometry on bead size and formability, we compared straight-through symmetric (rectangular duct, Fig. 2A) and asymmetric channels (cylinder with rectangular terrace, Fig. 2B) achieved by varying the channel width, height, and terrace depth (Table 1). We kept the aspect ratio of the outlet length/width to be over 5 assuming that a minimum aspect ratio is required to establish a unidirectional laminar flow [11]. Due to limitations in laser micro-machining, the walls of the ablated microchannels have a tapering angle ranging from 83 to 86° as the laser mills deeper into the plate, resulting in dimensional differences between the terrace inlet and the outlet widths. This occurs because of the shape of the focused laser

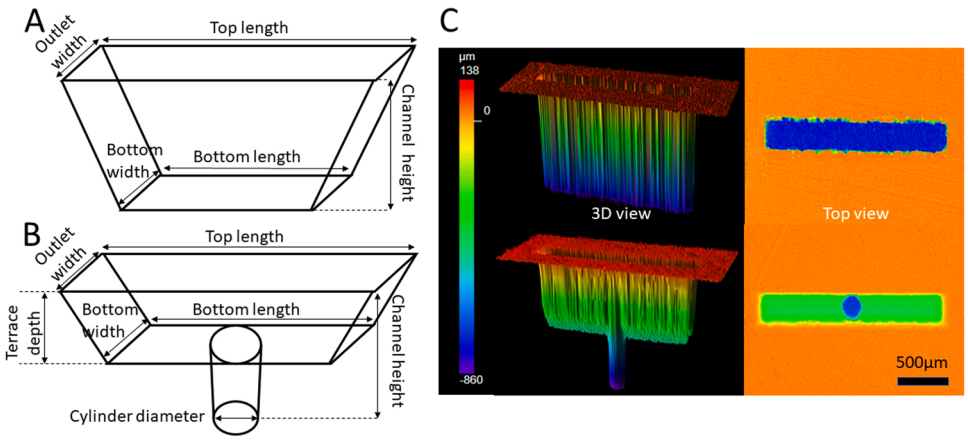

Fig. 2. Three-dimensional views of channel dimensions. (A) Symmetric channel dimensions., (B) Asymmetric channel dimensions. The length difference between the outlet and the inlet was exaggerated in the drawings to emphasize dimensional tapering. (C) Confocal heatmaps of two different channels.

Table 1
Dimensions and labels of channels used for the study. For most microchannels, only one channel was manufactured with the exception of Asym C (N > 20).

Channel type	Label	Rectangular duct length (μm) x width (μm)			Cylinder diameter (μm)	Hydraulic diameter at the inlet (μm)	Total channel height (μm)	Terrace depth if applicable (μm)
		Intended	Measured					
			Top	Bottom				
Symmetric	Sym A	2000 × 200	2350 × 514	2020 × 223	N/A	401	1635	NA
	Sym B	1500 × 150	1654 × 340	1362 × 126	N/A	188	860	NA
Asymmetric	Asym A	2000 × 250	2232 × 483	2130 × 350	320	320	1635	900
	Asym B	2000 × 200	2148 × 358	1850 × 242	238	238	1635	900
	Asym C	1500 × 150	1650 ± 70 × 300 ± 11	1525 ± 25 × 220 ± 10	210 ± 10	210 ± 10	860	500 ± 10
	Asym D	1500 × 150	2153 × 315	2073 × 235	220	220	860	275

beam, which forms a cone after passing through the focusing lens. (Table 1). Contrary to the terrace or duct, the cylinder orifice showed minimal dimensional tapering, potentially due to different laser-milling strategies used for each component. In contrast to the raster scan trajectory used for rectangular ablation, the laser beam spiraled in a circular shape to generate cylinder orifices. Due to the limitation of the focused laser beam's spot size, the minimum cylinder diameter achieved was 220 μm.

3.2. Superhydrophic channel surfaces obtained through laser micromilling

The microchannel surface should be as hydrophobic as possible to maximize oil phase wetting to promote droplet formation [19,29]. As expected [30], the hydrophobic pristine PTFE plates used for microchannel fabrication had water contact angles above 90° (advancing water contact angle of $\theta_A = 97 \pm 1°$; receding water contact angle of $\theta_R = 43 \pm 12°$). The laser irradiation process results in a hierarchical topography consisting of a rippled microstructure that is superimposed by porous, wiry nanostructures (Fig. 3A, B). This porous structure is known to trap air pockets, causing water to wet the surface in the Cassie-Baxter wetting state, leading to superhydrophobic behavior [31, 32]. Using a surrogate surface with an irradiated area large enough to deposit water drops, we measured dynamic water contact angles of $\theta_A = 150 \pm 4°$ and $\theta_R = 123 \pm 8°$ (Fig. 3C). These large contact angle measurements confirm that the irradiated PTFE has low water wetting properties, which is expected to aid in droplet-pinch off.

3.3. Heating and surfactant reduce bead coalescence

We applied a temperature gradient to the oil phase to avoid sudden temperature increase in the aqueous phase at the plate surface which could cause premature chitosan gelation and channel obstruction. Among the gelling agent formulations known in previous work [25], we chose a formulation of maximal stability at room temperature and rapid gelation at 37 °C (Supporting information Fig. S2). At higher phosphate concentrations, the precursor solution gelled too quickly, even at room temperature, resulting in generation of droplets with uncontrolled sizes as the overall processing time increases. At lower phosphate or carbonate concentrations, the gelation kinetics were too slow to obtain gelled beads in the collection reservoir.

Despite the temperature gradient established through this method, most droplets coalesced upon contact (Fig. 4 A). To stabilize the droplet interface and reduce coalescence during gelation, surfactants compatible with water-in-fluorocarbon oil emulsions were added in the oil. The surfactant we selected is a block copolymer of perfluoropolyether and polyethylene glycol widely used to stabilize water-in-fluorinated oil emulsions [33]. This surfactant is non-ionic which improves cytocompatibility compared to ionic fluorosurfactants [34]. The surfactant was effective in preventing bead coalescence at 0.066 % w/w, as shown in Fig. 4B. Also, Fluoro-Surfactants significantly reduced the interfacial tension between the two phases at this concentration in the pendant drop setting (oil-in-water), shown in Fig. 4 C.

As interfacial tension is one of the main driving forces in the droplet detachment process [15], we hypothesized that the surfactant concentration could potentially reduce the droplet size. However, the surfactant concentration had no significant effect on the average

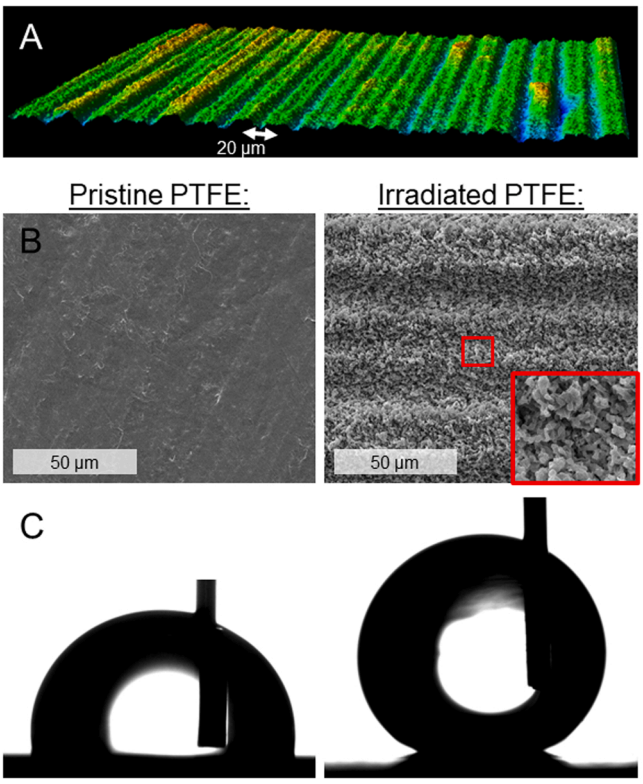

Fig. 3. Superhydrophobic properties of channel surfaces obtained by laser micromilling. (**A**) Confocal heatmap of the rippled microstructure. Ridges are spaced 20 μm apart. (**B**) Scanning electron micrographs of the pristine and laser irradiated PTFE. The red box in the irradiated image provides a magnified view of the nanostructure. (**C**) Images of the advancing water contact angle on pristine (left) and irradiated (right) PTFE.

volume-weighed bead diameter ($D_{4,3}$, De Brouckere diameter), as shown in Fig. 4D. Unlike the pendant drop setting where droplet detachment takes more than seconds, the detachment time in the microchannel (milliseconds) may be too short for the surfactants to affect the interfacial tension [35]. The rate of surfactant diffusion to the droplet interface may have been insufficient to impact droplet detachment while still creating a sufficient energy barrier to avoid later coalescence.

3.4. Asymmetric channels aid in reducing droplet size

To reduce diffusion distances and enable eventual in vivo delivery via needle injection, bead diameters of reduced size (≤600 μm) were desirable. The beads generated using two different channel geometries with relatively similar inlet/outlet width and height showed significant differences in average diameter (D_{43} 2222 ± 31 μm for Sym A, 1013 ± 10 μm for Asym A, Fig. 5). To determine whether a change in overall channel size could affect the bead diameter, we generated beads using channels with smaller inlet widths. For symmetric channels, a decrease in channel width showed no significant change in bead diameter (D_{43} 2222 ± 31 μm for Sym A, 2105 ± 57 μm for Sym B). As expected [11], reducing the terrace width of asymmetric channels led to a significant reduction in bead diameter (D_{43} 1013 ± 10 μm for Asym A, 573 ± 6 μm for Asym C). The ratio of resultant bead diameter to the inlet width exceeded 10 in symmetric channels, whereas the ratio was 2–3 for asymmetric channels. Considering that the aspect ratio of the terrace is over 5, the result might indicate that asymmetric channels could effectively pinch off a droplet before the droplet diameter expands to reach the channel length [35], which may not have been the case for the symmetric channel under the conditions applied. Comparing channels of different duct or terrace depth (Sym B: 0, Asym C: 500 μm, Asym D: 275 μm) indicated that a minimum depth was required in asymmetric channels to achieve effective droplet pinch-off and significantly reduce the bead diameter.

Larger (> 1500 μm) beads generated using symmetric channels tended to coalesce to form larger beads, likely due to incomplete gelation, resulting in bimodal or trimodal bead size distributions (C.V. > 20 %). In contrast, the beads produced by asymmetric channels showed distinctive uninomodal size distribution (C.V < 10 %). From here on, to further decrease the size of the beads, we focused on optimizing the system using the channel with the smallest width (Asym C).

3.5. Droplet sizes below 3-fold the channel width are obtained when interfacial tension forces are predominant

To study the effect of aqueous phase viscosity on bead diameter, we generated beads using precursor solutions with different chitosan concentrations at a fixed flow rate and quantified D_{43}. To avoid the changes of viscosity with time [25], we mixed chitosan with Milli-Q water instead of gelling agent. This measurement would represent a value near the initial pre-gelling viscosity of the chitosan mixture. The solution at the highest viscosity (2 % chitosan) generated broad bead size distributions. The dispersed solution often obstructed the channel leading to unstable flow observed as interruption in bead production followed by sporadic 'bursts' of rapid droplet formation. At 1.6 % chitosan concentration, uniform droplets were observed, but the size was abnormally large (1454 ± 28 μm) – over 5 times the rectangular terrace width. Conversely, the solution at the lowest viscosity (1.2 % chitosan) generated beads with a diameter of 600 ± 20 μm, which is roughly 2–3 times the width (Fig. 6 A).

To further investigate the trend in bead size associated with the aqueous phase viscosity, we applied dextran solutions of different concentration as another model system. In Fig. 6 A, the Regime 1 represents the region where the microchannel can consistently generate droplet sizes 2–3 times the rectangular duct width, whereas Regime 2 represents the region with droplet size over 5 times the width. The 1.2 % chitosan solution falls under the Regime 1 (Fig. 6 A). The system allows the production of small droplets regardless of viscosity under a critical value, which was within 30 – 58 mPa•s in the current context. Although 1.2 % chitosan precursor solution allowed stable generation of small droplets, beads obtained when adding gelling agent did not withstand the rinsing process. Therefore, based on size uniformity and stability after the encapsulation process, 1.6 % chitosan precursor solutions were used for process optimization towards cell encapsulation.

To identify the maximum flow rate that produces stable small-diameter droplets (Fig. 6B), we dispersed the precursor solution (1.6 % w/v chitosan) at different flow rates and quantified the droplet diameter as a function of *Ca* [19,36]. The *Ca* was calculated using $Ca = (U \bullet \eta)/\gamma$ (*Ca*: capillary number, *U*: average dispersed phase velocity at the channel entrance, η: dispersed phase viscosity, and γ: interfacial tension assumed to be 35 mN/m). As viscosity changes as a function of time, the value used in *Ca* calculations was the viscosity of the chitosan precursor solution without the gelling agent, which was assumed to represent the viscosity immediately after mixing. Shown in Fig. 6B, at flow rates below 0.02 mL/min ($Ca = 1.3 \times 10^{-2}$), the channel consistently generated small droplets (570 ± 50 μm) regardless of flow rate increase. When flow rates exceeded 0.03 mL/min, the average diameter abruptly increased as the flow rate increased. The corresponding Ca_c value lies between 1.3×10^{-2} to 2×10^{-2}, which is on the same order of magnitude as previous reports [37]. The *Ca* values for different chitosan precursor solution concentrations tested in Fig. 6 A are also consistent with the Ca_c value (1.2 % chitosan, 0.1 mL/min, $Ca = 0.01$, Regime 1; 1.6 % chitosan, 0.1 mL/min, $Ca = 0.05$, Regime 2).

3.6. Injectability

To determine whether the microchannel emulsification beads would

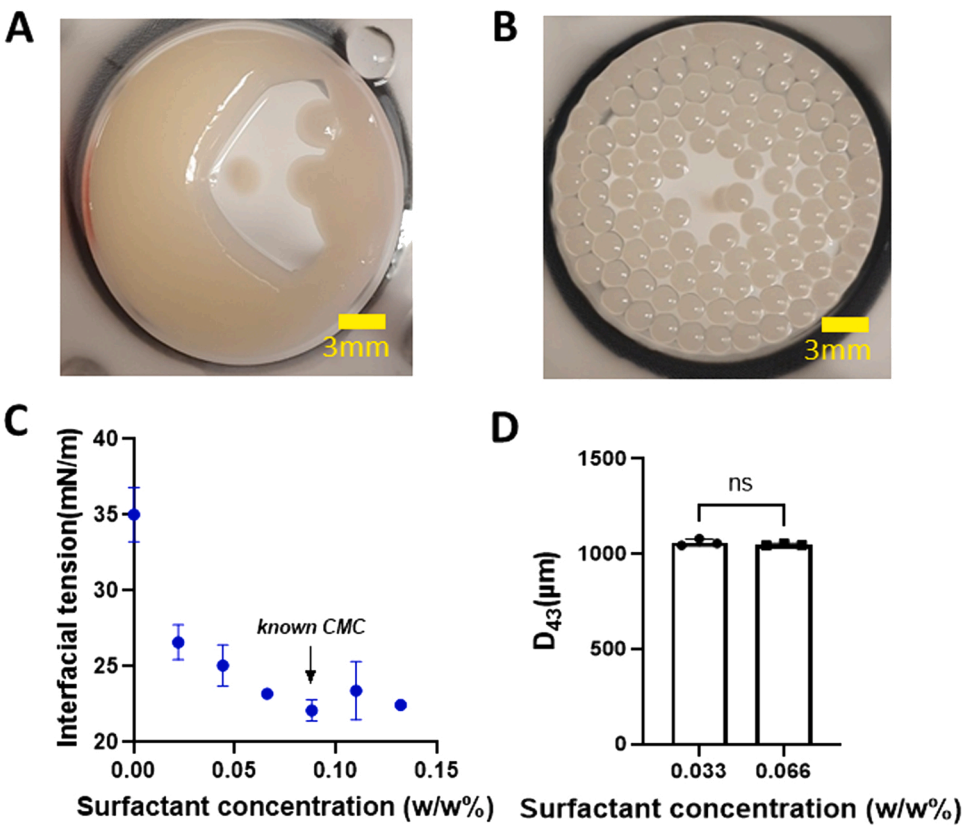

Fig. 4. Effect of fluorosurfactant on bead coalescence and the average bead size. (**A**) Coalesced droplets generated without surfactant. (**B**) Droplets floating in the oil phase at 22 C° with surfactant concentration of 0.066 % w/w. Both images were taken 1 min after the generation process. (**C**) Interfacial tension between the chitosan solution (1.6 % w/v) and the oil phase at different surfactant concentrations. (**D**) D_{43} of the beads generated at two different surfactant concentrations, critical micelle concentration (Critical micelle concentration, 0.066 % w/w) and 0.033 % w/w. (N = 3, n > 750). Asym A (Table 1) was used for droplet generation.

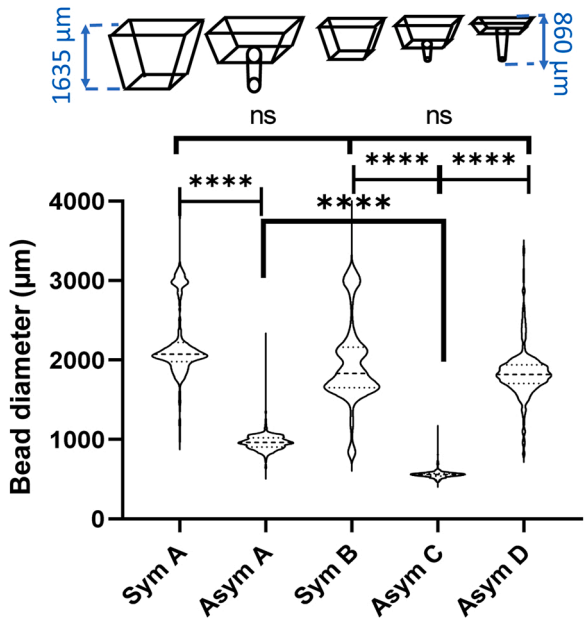

Fig. 5. Effect of channel geometry on bead size distribution. Size distribution of beads generated by channels of (1) different types (Sym A and Asym A) and (2) different slot depths (Sym B, Asym C, Asym D). See detailed dimensions in Table 1. Each dotted line within the violin plot marks the quantile point dividing the range of the percentage distribution. (N > 2, n > 750, **** = p < 0.0001).

be suitable for in vivo delivery, we compared their mechanical properties and resistance to passage through a needle to that of chitosan beads obtained through stirred emulsification. To allow side-by-side comparison, we generated stirred emulsification beads of matching $D_{4,3}$ by adjusting the agitation rate during the process. We chose $D_{4,3}$ as metric since this is representative of the conditions the average MSC, which are distributed uniformly within the bead volume, would experience. The $D_{4,3}$ of microchannel emulsification beads was 765 ± 16 μm with C.V. of 9 % ± 1 % compared to the $D_{4,3}$ of stirred emulsification beads was 729 ± 50 μm with C.V. of 41 % ± 5 %, as shown in Fig. 7.

To demonstrate improved injectability of beads with narrower size distribution, we infused the beads through a syringe needle that is slightly smaller in size (ID: 513 μm) compared to $D_{4,3}$. To quantify the number of ruptured beads at different bead densities, we prepared beads suspended in two different buffer volumes. At both concentrations, the fraction of ruptured microchannel emulsification beads was significantly lower than that of stirred emulsification beads, namely 20 % ± 5 % damaged beads/total beads compared to 39 % ± 6 % at high beads/buffer volume ratio (1/3), reduced to 5 % ± 5 % and 20 % ± 3 % respectively at higher dilution (1/6) (Fig. 8 A). Reducing bead concentration may have significantly impacted the rheology of the solution passing through the needle when beads were uniform in size, but this effect may not have been as impactful for beads of broad size distribution. The fraction of ruptured beads is based on bead numbers, and hence the large fraction of ruptured beads in stirred emulsification would represent an even larger volumetric fraction of inadequately encapsulated cells. We also infused the beads through a smaller needle of 23 G (ID:337 μm) to measure the injectable limit. Most beads ruptured after injection for both microchannel emulsification and stirred emulsification beads, making it difficult to quantify.

To further assess the mechanical properties of the beads, we used a parallel plate compression set-up to compress single beads of matching size (700–800 μm in diameter) up to 30 % in volume. The degree of volume compression was determined to match the inner diameter of the 21 G needle (513 μm) to the compressed bead height. No significant difference in compressive moduli was observed between microchannel emulsification and stirred emulsification beads, suggesting that the improved injectability of microchannel emulsification beads resulted

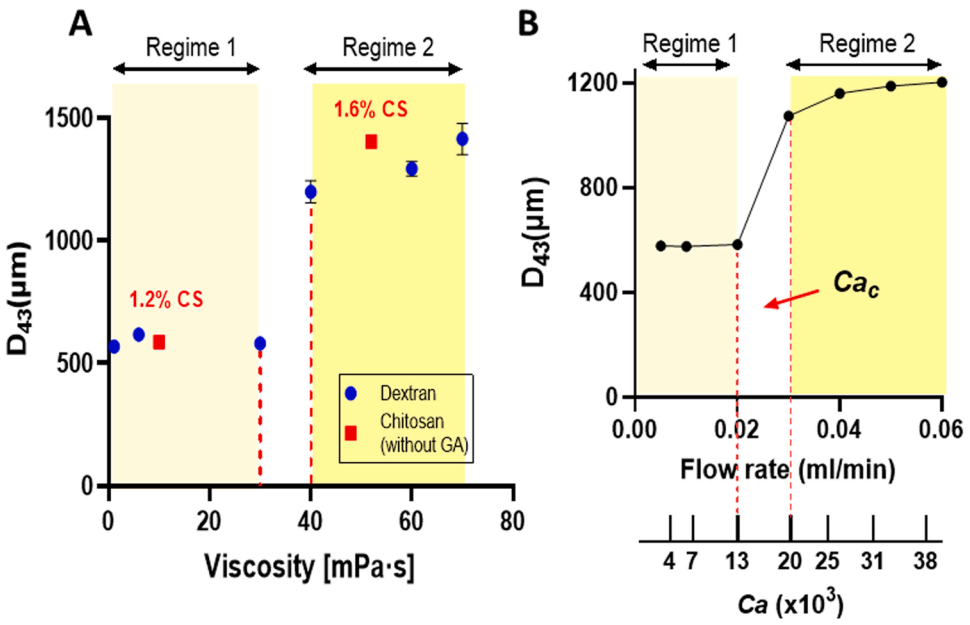

Fig. 6. Effect of aqueous phase viscosity & flow rate on bead size. (A) Difference in average bead size depending on the aqueous phase viscosity at a fixed flow rate (0.1 mL/min). Dextran (blue dots) concentration was increased from 0 g/mL to 0.33 g/mL. The apparent viscosity was measured at shear rate ranging from 10 to 400 (1/s), which is calculated to be the shear rate range in the cylinder channel at flow rate (0.05–0.10 mL/min). (B) Effect of flow rate on bead size at a fixed chitosan concentration (1.6 % w/v), (N = 3, n > 90). For both studies, Asym C was used. (Ca: Capillary number).

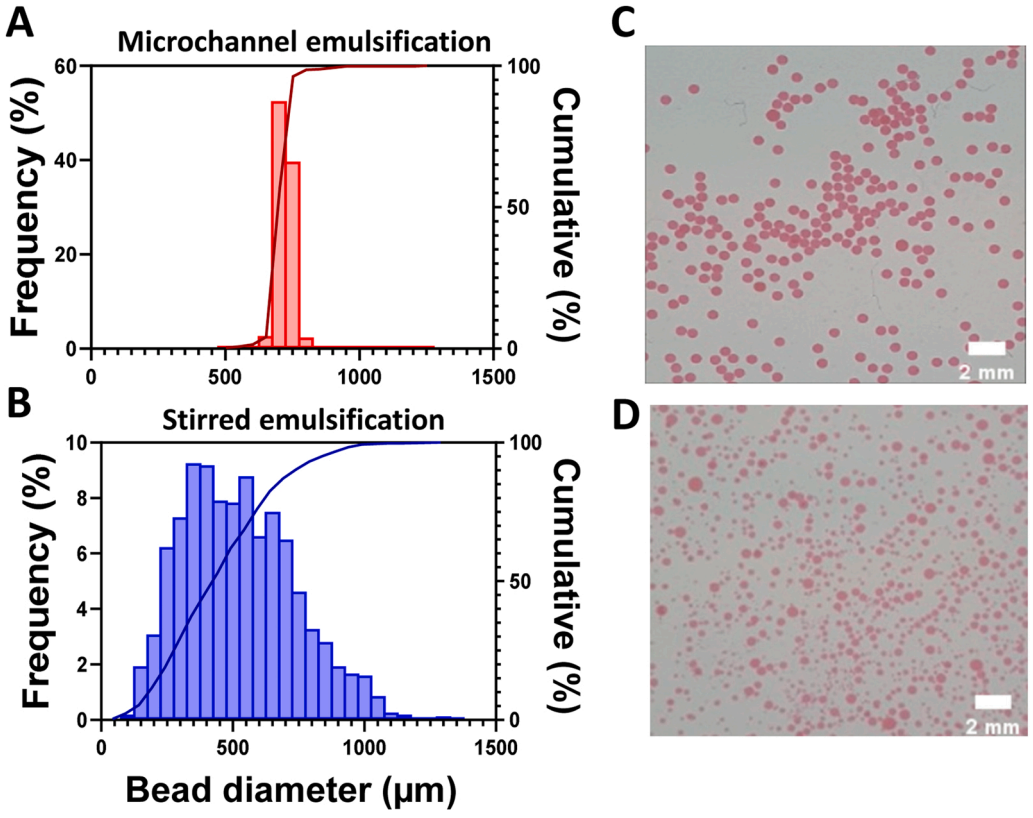

Fig. 7. Size distribution of chitosan microbeads generated by (A) microchannel emulsification or (B) stirred emulsification, and the representative images of the respective beads (**C, D**). For the aqueous phase, 1.6 % chitosan was used. To match the average size of microchannel emulsification beads, the stir speed was set to 600 rpm for stirred emulsification. (N = 3, n > 750).

from the absence of undesirably large microbeads in the batch. After a first compression cycle, slight plastic deformation was observed as the force showed a negative value. Nonetheless, microchannel emulsification beads withstood 30 % volume compression for three consecutive cycles without any rupture (Fig. 8C).

3.7. MSCs survive the encapsulation process and secrete VEGF

Next, we measured the viability and VEGF A secretion of MSCs after the bead production process to assess the suitability of the process for cell immobilization. VEGF A secretion was selected as a functional metric due to the key role of this growth factor in neovascularization [38]. MSCs showed high viability in both microchannel and stirred

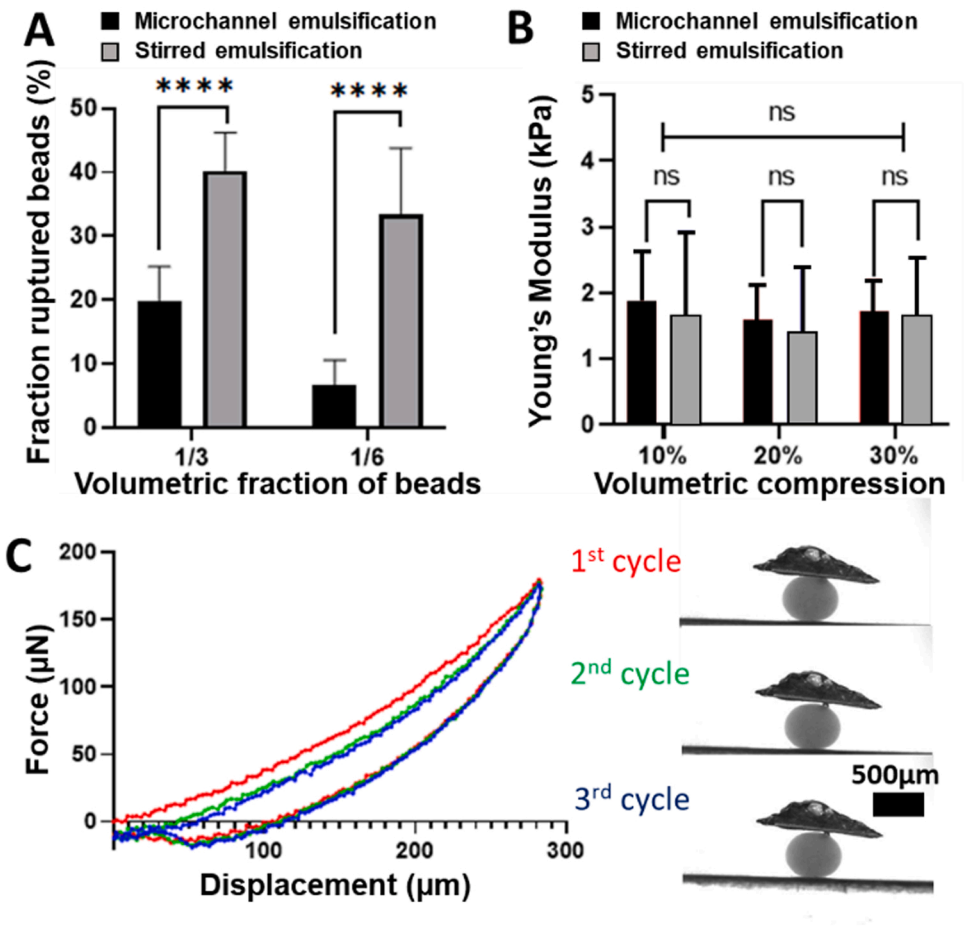

Fig. 8. Mechanical properties of chitosan beads generated by microchannel and stirred emulsification. (A) Percentage of beads ruptured after passing through a 21 G needle (ID: 513 μm). The beads were suspended in buffer at different dilutions prior to collection in a syringe and passage through the needle (N = 3, n > 20). (B) Compressive moduli of microbeads measured within 24 h after production (N = 3, n = 6). (C) Representative viscoelastic behavior of microchannel emulsification beads compressed up to 30 % volume for 3 cycles.

emulsification processes 1 h after encapsulation (Day 0), as shown in Fig. 9A, B. To reflect conditions required for eventual cytokine secretion and transplantation assays, the cells were incubated in alpha-MEM with 0.2 % FBS for 3 days. As expected in these low-serum conditions [39], the viability decreased over the following 3 days but no significant differences in cell survival nor VEGF secretion were observed between the microchannel and stirred emulsification beads (Fig. 9C). These results offer preliminary evidence that the microchannel emulsification process would be a suitable alternative to stirred emulsification for MSC encapsulation and delivery for ischemic tissue repair.

4. Discussion

In our previous study [19], we developed a microchannel emulsification device to immobilize pancreatic cell aggregates (MIN6 cells) in alginate microbeads. Here, both the cell type and gelation mechanisms were modified requiring device and process adaptation. Initially, the same channel geometry (symmetric channels) was used with chitosan as previously applied for alginate bead production. However, contrary to the alginate-based encapsulation process, where the droplets gel immediately after being detached from the channel, bead coalescence was observed since heat-induced gelation of chitosan is not instantaneous. To prevent droplet coalescence and to reach the target bead diameter (~600 μm to allow needle injection), we added fluorosurfactant and reduced the bead size significantly using asymmetric channels. It was assumed that the cylindrical shaft of the asymmetric channel limited the volume of the aqueous phase entering into the channel, while the large aspect ratio of the terrace allowed oil inflow prior to droplet formation and constricted the droplet neck as the aqueous phase exited the shaft [35].

Due to the dimensional tapering during laser micromachining, it was difficult to produce a channel size (inlet cylindrical diameter) smaller than 220 μm for asymmetric channels. As the channel size decreased, smaller droplets formed which accelerated heat transfer and hence gelation. This improved bead stability in the collection compartment, but also led to increased time-dependent changes in viscosity affecting the dependence of bead size and process stability on flow rate. To improve process robustness, we studied the effect of aqueous phase viscosity and flow rate, and hence Ca, on bead size and process stability (uninterrupted bead production). Since the viscosity of the chitosan precursor solution changed over time during dispersion, it was crucial to determine Ca_c and make necessary changes in either the viscosity or the flow rate.

The device also went through structural changes. The volume of aqueous phase required to fill the bottom chamber before dispersion through a channel was reduced from 9 mL to 1.5 mL to minimize the aqueous phase dead volume. The second outlet in the bottom chamber previously designed to prevent pressure build-up was removed as the pressure loss through the outlet could cause bead production instability. To reduce the probability of early bead-bead contact in the collection vessel, the surface area of the collection site was increased from 60 cm^2 to 120 cm^2. By using a fluorosurfactant, adapting channel and device geometry, as well as changing process variables, we were able to produce uniform-size chitosan beads (C.V < 10 %) of diameters below 600 μm without incurring coalescence. When cells were added in the precursor solution, the bead size obtained increased to ~750 μm likely due to increases in viscosity associated with the presence of cells. We observed intermittent channel obstruction or production of abnormally large droplets 30 min after the initial aqueous phase dispersion during the cell encapsulation. To maintain the size uniformity of a batch, the

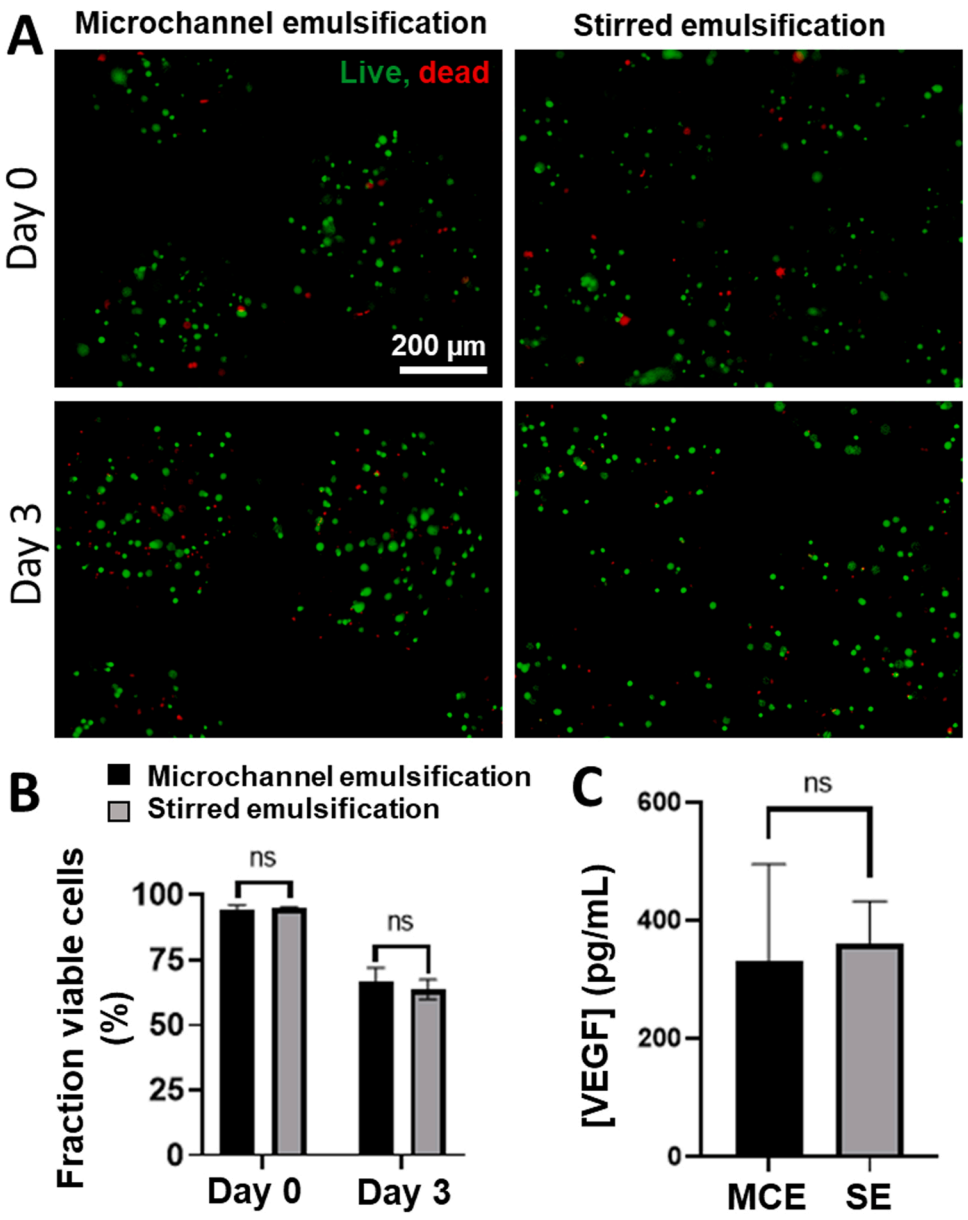

Fig. 9. Cytocompatibility of microchannel and stirred emulsification beads. (A) Representative fluorescence images of hMSCs in microchannel emulsification or stirred emulsification beads after calcein AM (live) and ethidium homodimer (dead) staining. (B) Quantification of cell viability for each process at day 0 and after 3 days of culture (>1000 cells per sample; N = 3). (C) VEGF release in culture media after 3 days of culture in chitosan microbeads (N = 3). MCE: microchannel emulsification; SE: stirred emulsification.

production time was limited to ensure that the viscosity change during the process did not reach values leading to changes in droplet formation regime. While maintaining improved size uniformity and injectability, no significant difference in cell viability and VEGF secretion was observed compared to the previous method (stirred emulsification).

4.1. *Impact and future directions*

The objective of this research was to develop and optimize a microchannel emulsification method for the fabrication of chitosan hydrogel microbeads with control over process stability, bead size, bead mechanical properties, and viability of encapsulated cells. The microchannel emulsification device was successfully adapted for the thermoresponsive chitosan-based gelation process by redesigning the device and providing a temperature gradient in the oil phase. Coalescence of smaller (<1500 μm diameter) beads was prevented by adding surfactants, allowing production of chitosan beads of uniform size with high MSC survival after the process. Although we did not observe any detrimental impact on cell viability and cell secretion during our study, the beads generated with fluorosurfactants should be investigated in terms of their cytotoxicity, fibrotic responses post-transplantation and therapeutic outcomes of the encapsulated cells.

A significant advantage of microchannel emulsification over stirred emulsification-based encapsulation of MSCs for cell therapy applications is size uniformity. This was demonstrated through the coefficient of variation (< 10 % versus > 40 % respectively) and through the reduction in the fraction of damaged beads after passage through a 21 G needle. The reduction in bead rupture was not attributed to differences in compressive modulus, as no significant differences between microchannel emulsification and stirred emulsification beads were observed for this metric. Rather, the fraction of beads of significantly larger diameter than the needle was higher with stirred emulsification for matched $D_{4,3}$ values. Size uniformity is also expected to reduce heterogeneity in oxygen and other nutrient gradients, leading to more uniform anticipated in vivo performance. Size uniformity may also lead to more consistent lysozyme-drive degradation rates between beads post-transplantation [40].

The main parameter controlling the bead diameter are microchannel geometry and dimensions. Further reduction in the bead diameter could be achieved by using a laser setup that can minimize dimension tapering

to generate channels with smaller terrace widths (< 100 μm). Channel tapering could also be reduced by creating a precise system to mill channels from both sides. In parallel, the aqueous phase viscosity and flow rate should be further adjusted to let the system *Ca* fall under the stable processing zone. Integrating temperature-controlled zones within the device could further improve control over chitosan gelation kinetics.

Microchannel emulsification can readily be scaled up through milling of hundreds or thousands of channels through a single plate [41]. Current device dimensions would allow incorporation of at least 50 microchannels, with current throughput of 6 mL/h/channel. Throughput of this magnitude would be challenging to achieve with microfluidic technologies previously applied for drug immobilization in chitosan microbeads [42]. To achieve higher flow rates and reduce viscosity changes during processing, multiple channels can be created in a single PTFE plate to promote simultaneous bead production at each channel. The system should also be optimized to establish a stable bead production at higher cell density, considering that many clinical applications require cell density over 10^6 cells/mL hydrogel to promote tissue regeneration [39,43]. These efforts should account for the viscosity rise and changes in Ca values resulting from the cell density increase. The effect of different chitosan formulations on the MSC secretome and in vivo retention at the delivery site should be investigated to maximize their immunomodulatory, angiogenic and other therapeutic effects.

5. Conclusions

This work describes the novel application of microchannel emulsification to mammalian cell encapsulation in chitosan physical hydrogel beads formed through thermoresponsive gelation. Process parameters were adjusted to generate monodisperse chitosan beads of controlled size ranging from 600 to 1500 μm in diameter while maintaining high MSC post-encapsulation viability (95 %). Compared to stirred emulsification, fewer beads ruptured when passing through a needle of similar diameter as the average bead diameter – as expected from the narrower bead size distribution of the microchannel beads. No significant differences between the stirred and microchannel emulsification beads were observed when considering mechanical properties, MSC process survival or VEGF secretion. Microchannel emulsification is a powerful new approach to encapsulate mammalian cells in hydrogels that undergo temperature-sensitive gelation.

CRediT authorship contribution statement

Dongjin S. Shin: Conceptualization, Methodology, Software, Validation, Formal analysis, Investigation, Data curation, Writing – original draft, Writing – review and editing, Visualization, **Francesco K. Touani:** Conceptualization, Methodology, Validation, Formal analysis, Investigation, Data curation, Writing – original draft, Writing – review and editing, Visualization. **Damon G.K. Aboud:** Methodology, Software, Validation, Investigation, Writing – original draft, Writing – review and editing, Visualization, **Anne-Marie Kietzig:** Methodology, Resources, Formal analysis, Writing – review and editing, Supervision, **Sophie Lerouge:** Conceptualization, Methodology, Formal analysis, Data curation, Writing – review and editing, Supervision, Project administration, Funding acquisition. **Corinne A. Hoesli:** Conceptualization, Methodology, Formal analysis, Data curation, Writing – review and editing, Supervision, Project administration, Funding acquisition.

Declaration of Competing Interest

The authors declare no competing interests.

Data Availability

Data will be made available on request.

Acknowledgements

We thank Balaji Ramachandran and Jonathan Brassard for valuable discussions. Dr. Ramachandran also conducted interfacial tension measurements with Dongjin Shin. This study was funded by the Quebec Cell, Tissue and Gene Therapy Network –ThéCell (a thematic network supported by the Fonds de recherche du Québec–Santé). The work was also supported by grants from the Canada Foundation for Innovation (35507), and the Natural Sciences and Engineering Research Council of Canada (C.H.: RGPIN-2020-05877, S.L.: RGPIN-2020-06684). This research was undertaken, in part, thanks to funding from the Canada Research Chairs Program. Dongjin Shin was supported by Eugenie Ulmer-Lamothe awards from the Department of Chemical Engineering, McGill University. Several other research networks provided training and collaboration opportunities, including the McGill Regenerative Medicine Network, the Québec Center for Advanced Materials, The Quebec Network for Research on Protein Function, Engineering, and Applications – PROTEO, the Cardiometabolic Health, Diabetes and Obesity Research Network, Canada's Stem Cell Network, the Canadian Biomaterials Society and the Bioencapsulation Research Group.

Appendix A. Supporting information

Supplementary data associated with this article can be found in the online version at doi:10.1016/j.colsurfa.2022.130807.

References

[1] U. Prusse, L. Bilancetti, M. Bucko, B. Bugarski, J. Bukowski, P. Gemeiner, D. Lewinska, V. Manojlovic, B. Massart, C. Nastruzzi, V. Nedovic, D. Poncelet, S. Siebenhaar, L. Tobler, A. Tosi, A. Vikartovska, K.D. Vorlop, Comparison of different technologies for alginate beads production, Chem. Pap. 62 (2008) 364–374.
[2] C.A. Hoesli, R.L. Kiang, D. Mocinecova, M. Speck, D.J. Moskova, C. Donald-Hague, I. Lacik, T.J. Kieffer, J.M. Piret, Reversal of diabetes by betaTC3 cells encapsulated in alginate beads generated by emulsion and internal gelation, J. Biomed. Mater. Res B Appl. Biomater. 100 (2012) 1017–1028.
[3] C.A. Hoesli, R.L.J. Kiang, K. Raghuram, R.G. Pedroza, K.E. Markwick, A.M. R. Colantuoni, J.M. Piret, Mammalian cell encapsulation in alginate beads using a simple stirred vessel, J. Vis. Exp. (2017).
[4] C.A. Hoesli, K. Raghuram, R.L. Kiang, D. Mocinecova, X. Hu, J.D. Johnson, I. Lacik, T.J. Kieffer, J.M. Piret, Pancreatic cell immobilization in alginate beads produced by emulsion and internal gelation, Biotechnol. Bioeng. 108 (2011) 424–434.
[5] Y. Alinejad, C.M.E. Bitar, K. Martinez Villegas, S. Perignon, C.A. Hoesli, S. Lerouge, Chitosan microbeads produced by one-step scalable stirred emulsification: a promising process for cell therapy applications, ACS Biomater. Sci. Eng. 6 (2020) 288–297.
[6] W.H. Tan, S. Takeuchi, Monodisperse alginate hydrogel microbeads for cell encapsulation, Adv. Mater. 19 (2007) 2696.
[7] V.L. Workman, S.B. Dunnett, P. Kille, D.D. Palmer, Microfluidic chip-based synthesis of alginate microspheres for encapsulation of immortalized human cells, Biomicrofluidics 1 (2007) 14105.
[8] L. Capretto, S. Mazzitelli, G. Luca, C. Nastruzzi, Preparation and characterization of polysaccharidic microbeads by a microfluidic technique: application to the encapsulation of Sertoli cells, Acta Biomater. 6 (2010) 429–435.
[9] H. Huang, Y. Yu, Y. Hu, X. He, O. Berk Usta, M.L. Yarmush, Generation and manipulation of hydrogel microcapsules by droplet-based microfluidics for mammalian cell culture, Lab Chip 17 (2017) 1913–1932.
[10] L.M. Caballero Aguilar, S. Duchi, C. Onofrillo, C.D. O'Connell, C. Di Bella, S. E. Moulton, Formation of alginate microspheres prepared by optimized microfluidics parameters for high encapsulation of bioactive molecules, J. Colloid Interface Sci. 587 (2021) 240–251.
[11] I. Kobayashi, M.A. Neves, Y. Wada, K. Uemura, M. Nakajima, Large microchannel emulsification device for mass producing uniformly sized droplets on a liter per hour scale, Green Processing and Synthesis 1 (2012) 353–362.
[12] K.C. van Dijke, K.C. Schroen, R.M. Boom, Microchannel emulsification: from computational fluid dynamics to predictive analytical model, Langmuir 24 (2008) 10107–10115.
[13] I. Kobayashi, S. Mukataka, M. Nakajima, CFD simulation and analysis of emulsion droplet formation from straight-through microchannels, Langmuir 20 (2004) 9868–9877.
[14] E. van der Zwan, R. van der Sman, K. Schroen, R. Boom, Lattice Boltzmann simulations of droplet formation during microchannel emulsification, J. Colloid Interface Sci. 335 (2009) 112–122.
[15] S. Sugiura, M. Nakajima, T. Oda, M. Satake, M. Seki, Effect of interfacial tension on the dynamic behavior of droplet formation during microchannel emulsification, J. Colloid Interface Sci. 269 (2004) 178–185.

[16] E. Amstad, M. Chemama, M. Eggersdorfer, L.R. Arriaga, M.P. Brenner, D.A. Weitz, Robust scalable high throughput production of monodisperse drops, Lab Chip 16 (2016) 4163–4172.
[17] G.T. Vladisavljevic, I. Kobayashi, M. Nakajima, Effect of dispersed phase viscosity on maximum droplet generation frequency in microchannel emulsification using asymmetric straight-through channels, Microfluid Nanofluid 10 (2011) 1199–1209.
[18] S. Sugiura, T. Oda, Y. Izumida, Y. Aoyagi, M. Satake, A. Ochiai, N. Ohkohchi, M. Nakajima, Size control of calcium alginate beads containing living cells using micro-nozzle array, Biomaterials 26 (2005) 3327–3331.
[19] C.M.E. Bitar, K.E. Markwick, D. Trelova, Z. Kronekova, M. Pelach, C.M.O. Selerier, J. Dietrich, I. Lacik, C.A. Hoesli, Development of a microchannel emulsification process for pancreatic beta cell encapsulation, Biotechnol. Prog. 35 (2019), e2851.
[20] L. Gasperini, J.F. Mano, R.L. Reis, Natural polymers for the microencapsulation of cells, J. R. Soc. Interface 11 (2014) 20140817.
[21] K. Sakai, R. Katsumi, A. Isobe, F. Nanjo, Purification and hydrolytic action of a chitosanase from Nocardia orientalis, Biochim Biophys. Acta 1079 (1991) 65–72.
[22] S. Islam, M.A.R. Bhuiyan, M.N. Islam, Chitin and Chitosan: structure, properties and applications in biomedical engineering, J. Polym. Environ. 25 (2016) 854–866.
[23] A. Chenite, C. Chaput, D. Wang, C. Combes, M.D. Buschmann, C.D. Hoemann, J. C. Leroux, B.L. Atkinson, F. Binette, A. Selmani, Novel injectable neutral solutions of chitosan form biodegradable gels in situ, Biomaterials 21 (2000) 2155–2161.
[24] E. Assaad, M. Maire, S. Lerouge, Injectable thermosensitive chitosan hydrogels with controlled gelation kinetics and enhanced mechanical resistance, Carbohydr. Polym. 130 (2015) 87–96.
[25] C. Ceccaldi, E. Assaad, E. Hui, M. Buccionyte, A. Adoungotchodo, S. Lerouge, Optimization of injectable thermosensitive scaffolds with enhanced mechanical properties for cell therapy, Macromol. Biosci. 17 (2017) 1600435.
[26] J.D. Berry, M.J. Neeson, R.R. Dagastine, D.Y. Chan, R.F. Tabor, Measurement of surface and interfacial tension using pendant drop tensiometry, J. Colloid Interface Sci. 454 (2015) 226–237.
[27] C.A. Schneider, W.S. Rasband, K.W. Eliceiri, NIH Image to ImageJ: 25 years of image analysis, Nat. Methods 9 (2012) 671–675.
[28] K. Kim, J. Cheng, Q. Liu, X.Y. Wu, Y. Sun, Investigation of mechanical properties of soft hydrogel microcapsules in relation to protein delivery using a MEMS force sensor, J. Biomed. Mater. Res A 92 (2010) 103–113.
[29] I. Kobayashi, M. Nakajima, S. Mukataka, Preparation characteristics of oil-in-water emulsions using differently charged surfactants in straight-through microchannel emulsification, Colloids Surf. a-Physicochem. Eng. Asp. 229 (2003) 33–41.
[30] M.J. Wood, F. Aristizabal, M. Coady, K. Nielson, P.J. Ragogna, A.M. Kietzig, The precise and accurate production of millimetric water droplets using a superhydrophobic generating apparatus, Phys. Fluids 30 (2018), 027104.
[31] F. Liang, J. Lehr, L. Danielczak, R. Leask, A.M. Kietzig, Robust non-wetting PTFE surfaces by femtosecond laser machining, Int J. Mol. Sci. 15 (2014) 13681–13696.
[32] D.G.K. Aboud, A.-M. Kietzig, Splashing threshold of oblique droplet impacts on surfaces of various wettability, Langmuir 31 (2015) 10100–10111.
[33] M.S. Chowdhury, W. Zheng, S. Kumari, J. Heyman, X. Zhang, P. Dey, D.A. Weitz, R. Haag, Dendronized fluorosurfactant for highly stable water-in-fluorinated oil emulsions with minimal inter-droplet transfer of small molecules, Nat. Commun. 10 (2019) 4546.
[34] C. Holtze, A.C. Rowat, J.J. Agresti, J.B. Hutchison, F.E. Angile, C.H. Schmitz, S. Koster, H. Duan, K.J. Humphry, R.A. Scanga, J.S. Johnson, D. Pisignano, D. A. Weitz, Biocompatible surfactants for water-in-fluorocarbon emulsions, Lab Chip 8 (2008) 1632–1639.
[35] I. Kobayashi, G.T. Vladisavljevic, K. Uemura, M. Nakajima, CFD analysis of microchannel emulsification: droplet generation process and size effect of asymmetric straight flow-through microchannels, Chem. Eng. Sci. 66 (2011) 5556–5565.
[36] N. Khalid, I. Kobayashi, K. Uemura, M. Nakajima, Asymmetrical microchannel emulsification plates for production of small-sized monodispersed emulsion droplets, Chem. Eng. Technol. 40 (2017) 2351–2355.
[37] S. Sugiura, M. Nakajima, N. Kumazawa, S. Iwamoto, M. Seki, Characterization of spontaneous transformation-based droplet formation during microchannel emulsification, J. Phys. Chem. B 106 (2002) 9405–9409.
[38] W. Shi, Q. Xin, R. Yuan, Y. Yuan, W. Cong, K. Chen, Neovascularization: the main mechanism of MSCs in ischemic heart disease therapy, Front Cardiovasc Med 8 (2021), 633300.
[39] F.K. Touani, M. Borie, F. Azzi, D. Trudel, N. Noiseux, S. Der Sarkissian, S. Lerouge, Pharmacological preconditioning improves the viability and proangiogenic paracrine function of hydrogel-encapsulated mesenchymal stromal cells, Stem Cells Int 2021 (2021) 6663467.
[40] J.A. Jennings, Controlling chitosan degradation properties in vitro and in vivo, in: J.A. Jennings, J.D. Bumgardner (Eds.), Chitosan Based Biomaterials, Volume 1, Woodhead Publishing, 2017, pp. 159–182.
[41] N. Khalid, I. Kobayashi, M.A. Neves, K. Uemura, M. Nakajima, Microchannel emulsification: a promising technique towards encapsulation of functional compounds, Crit. Rev. Food Sci. Nutr. 58 (2018) 2364–2385.
[42] K.L. Ly, P. Hu, L.H.P. Pham, X. Luo, Flow-assembled chitosan membranes in microfluidics: recent advances and applications, J. Mater. Chem. B 9 (2021) 3258–3283.
[43] J.K. Wise, A.I. Alford, S.A. Goldstein, J.P. Stegemann, Comparison of uncultured marrow mononuclear cells and culture-expanded mesenchymal stem cells in 3D collagen-chitosan microbeads for orthopedic tissue engineering, Tissue Eng. Part A 20 (2014) 210–224.